Quaternary Science Reviews 210 (2019) 113–124

Contents lists available at ScienceDirect

Quaternary Science Reviews

journal homepage: www.elsevier.com/locate/quascirev

A new speleothem record of the penultimate deglacial: Insights into spatial variability and centennial-scale instabilities of East Asian monsoon

Gang Xue [a, b], Yanjun Cai [a, c, d, e, *], Le Ma [a], Xing Cheng [a, b], Hai Cheng [e, f], R. Lawrence Edwards [f], Dong Li [a, b], Liangcheng Tan [a, c, d, e]

[a] State Key Laboratory of Loess and Quaternary Geology, Institute of Earth Environment, Chinese Academy of Sciences, Xi'an, 710061, China
[b] University of Chinese Academy of Sciences, Beijing, 100049, China
[c] CAS Center for Excellence in Quaternary Science and Global Change, Xi'an, 710075, China
[d] Open Studio for OCCEC, Qingdao National Laboratory for Marine Science and Technology, Qingdao, China
[e] Institute of Global Environmental Change, Xi'an Jiaotong University, Xi'an, 710049, China
[f] Department of Earth Sciences, University of Minnesota, Minneapolis, MN, 55455, USA

ARTICLE INFO

Article history:
Received 1 October 2018
Received in revised form
15 February 2019
Accepted 20 February 2019
Available online 14 March 2019

Keywords:
Stalagmite
Oxygen isotope
Penultimate deglaciation
Weak monsoon interval
Coastline shift

ABSTRACT

We present a highly resolved oxygen isotope ($\delta^{18}O$) record of the penultimate glacial-interglacial transition from a ^{230}Th-dated stalagmite (SD1) from the Shangxiaofeng Cave in north-eastern China. Our $\delta^{18}O$ record reveals two prominent features. First, the SD1 $\delta^{18}O$ record documents a brief increase of $\delta^{18}O$ between 128.5 and 128.1 ka BP. Though this event has been identified in several marine records, our radiogenic dated record precisely constraints the timing and duration of the climate deterioration suggesting that this YD-like event is likely an intrinsic feature of climate change during the ice age terminations. Additionally, the $\delta^{18}O$ magnitude of the glacial-interglacial change (~0.7‰) is significantly smaller compared to the $\delta^{18}O$ records from inland and relatively high elevation caves (Dongge, Sanbao and Yangkou caves) (1.4–2.4‰) but comparable to the Hulu Cave at low elevation and proximal to the shallow Bohai and Yellow seas (Kelly et al., 2006; Cheng et al., 2006; Wang et al., 2008; Cheng et al., 2009; Li et al., 2014). Assuming that the cave $\delta^{18}O$ records mainly reflect precipitation isotope composition changes, the glacial-interglacial speleothem $\delta^{18}O$ difference between the various Chinese caves could be related to changes in atmospheric circulations, changing effect of altitude between the various caves and climate mean states, and large-scale changes in regional land-sea coverage due to sea level changes. The latter leads to disappearance and expansion of Bohai and Yellow seas during glacial and interglacial episodes, respectively, and likely affect the amount and isotope composition of precipitation. Taken together, our study highlights that hydroclimate imprints of the East Asian Monsoon changes during the penultimate glacial-interglacial cycle were spatially heterogeneous and centennial-scale monsoonal hydroclimate instabilities are likely inherent features of deglacial climate transition.

1. Introduction

Various archives are used to understand past Asian monsoon changes. Of these, speleothem has been proved to be one of the most important archives for studying the monsoonal climate changes in China (Cai et al., 2015; Cheng et al., 2009, 2016; Wang et al., 2008). The analysis of stable oxygen isotope in speleothems and its application as a proxy for changes in precipitation isotope composition has substantially broadened our understanding of Asian monsoon changes from orbital to decadal timescales. The results reveal that the variation of Asian monsoon is closely linked to changes in ice volume, orbital geometry, Atlantic Meridional Overturning Circulation, tropical sea surface temperature, solar activity and volcanic eruption (Anchukaitis et al., 2010; Cai et al., 2015; Cheng et al., 2009; Stager et al., 2011; Wang et al., 2001, 2005) on different timescales. However, most of these records are located in southern China and but only a few records from

* Corresponding author. State Key Laboratory of Loess and Quaternary Geology, Institute of Earth Environment, Chinese Academy of Sciences, Xi'an, 710061, China.
E-mail address: yanjun_cai@ieecas.cn (Y. Cai).

https://doi.org/10.1016/j.quascirev.2019.02.023
0277-3791/

northeast China have been reported, limiting our understanding of spatial variability and patterns of changes in paleohydroclimate.

At the same time, the interpretation of speleothem $\delta^{18}O$ as a proxy for rainfall changes is still in debate. In early studies, the speleothem $\delta^{18}O$, which largely record the precipitation oxygen isotope composition, has been interpreted as the 'ratio of the amount of summer to winter precipitation' or 'the relative summer to winter monsoon intensities' (Wang et al., 2001; Cheng et al. 2006, 2009), and as 'the fraction of water vapor removed from air masses between the tropical Indo-Pacific and southeastern China' (Yuan et al., 2004). These interpretations link the cave $\delta^{18}O$ with the Asian summer monsoon intensity (Wang et al., 2005; Zhang et al., 2008; Dykoski et al., 2005; Kelly et al., 2006; Cosford et al., 2008; Cai et al., 2006). However, some have argued that it might reflect the changes of moisture sources from different oceans, such as Pacific Ocean and South China Sea, and Indian Ocean (Maher, 2008; Dayem et al., 2010; Clemens et al., 2010). Recently, the speleothem record from southwest China documents not only 23-kyr precessional cycles punctuated by prominent millennial scale weak monsoon events synchronous with Heinrich events in the North Atlantic, but also clear glacial–interglacial variations that are consistent with marine records (Cai et al., 2015). This record also reveals that precipitation $\delta^{18}O$ difference on glacial-interglacial time scale in Indian summer monsoon region differs from southern China. This finding highlights that sea-level changes and related coastline shifts also likely contribute to the distinct disparity of precipitation $\delta^{18}O$ on glacial-interglacial timescale. However, this assumption still needs to be testified due to the complexity in the interpretation of precipitation $\delta^{18}O$ in East China.

Furthermore, the deglaciation is a period of major climate change, when Earth transitioned from its full glacial state to the interglacial climate. It presents a host of exciting opportunities to understand what factors control ice age cycles and to what extent the termination affects the global climate, and to try to understand a range of abrupt climate changes from decadal to millennial timescales within the context of more gradual trends. Many studies have disclosed the timing and variability of the abrupt climate changes within the deglaciation and found the similarities and dissimilarities between different deglaciations (e.g., the last deglaciation and penultimate deglaciation, Martrat et al., 2014; Jiménez-Amat and Zahn, 2015; Marino et al., 2015) and different regions (e.g., Europe and Asian monsoon region, Hauselmann et al., 2015). To this day, it is still unclear whether or not the centennial to millennial scales oscillations are the intrinsic feature of the deglaciation climate, due to the scarcity of well-dated high-resolution proxy records spanning the penultimate or even earlier deglaciations.

The climate on Shandong peninsula, the largest peninsula in China, is climatically dictated by East Asian monsoons, which is indispensable for the livelihood and sustainable development of this densely populated region, a traditional agricultural production area in China (Lu et al., 2011). Reconstructing the history and variability of past monsoon precipitation and understanding the forcing mechanisms are key to improve the capability of climate model simulation to project future climate changes (Kutzbach and Liu, 1997; Clemens et al., 1991). Moreover, Shandong peninsula is bordered by the Bohai Sea and Yellow Sea in East Asia, two marginal seas with less than 100 m water depth at present time. As continental ice sheets built up and sea level fell down, the coastline shifted southeast, and likely shifted 800–1000 km during the last glacial maximum when sea level was ~120m lower than at present time (Wang et al., 1997). This tremendous shift of coastline could have substantial impacts on the climate at Shandong peninsula, making it an ideal place to study the influence of coastline shift on the precipitation and its stable isotope composition.

Here, we present a high-resolution and precisely dated speleothem isotope record from the Shandong peninsula in northern China and reconstruct the history of precipitation $\delta^{18}O$ spanning the penultimate deglaciation in the study region. Our study aims to understand the regional variation of precipitation $\delta^{18}O$ and its linkage to the Asian summer monsoon and sea-level changes during the penultimate deglaciation in northern China, and to investigate the abrupt centennial-scale climate events during the penultimate deglaciation and their dynamic connections.

2. Cave site, local climate, materials and methods

The Shangxiaofeng Cave (36°21′N, 118°01′E, ~560m above sea level) is located 50 km south of Zibo city, Shandong Province, China (Fig. 1). The regional climate is typical monsoon climate of lower mid-latitude, characterized by hot and rainy summers, and by cold and dry winters. The annual precipitation is 736.6 mm and annual mean temperature is 13.6 °C, as recorded by nearby Boshan meteorological station, Shandong Province during the period from 1981 to 2010 AD. At the cave site, the summer monsoon brings warm and moist air during June, July and August and delivers 62% of annual precipitation, while moisture transported by continental air mass and moisture from eastern ocean (i.e. Bohai Sea and Yellow Sea) account for 38% of annual precipitation during the non-summer monsoon seasons (Wang et al., 2016).

The stalagmite SD-1 was collected from the inner chamber of the cave, about 150 m from the entrance. It is ~41 cm in length and ~12 cm in diameter. The stalagmite was halved along the growth axis by using a diamond saw and then polished (Fig. 2). Subsamples for ^{230}Th dating were drilled paralleled to the growth layers of the stalagmite at different depths (~75 mg per sample), and were dated at the Isotope Laboratory, Xi'an Jiaotong University using a Thermo-Fisher NEPTUNE multi-collection inductively coupled plasma mass spectrometer (MC-ICP-MS). The chemical procedures used to separate the uranium and thorium for ^{230}Th dating are similar to those described in Edwards et al. (1987), and the measuring protocol is the same as the one used by Cheng et al. (2013). A $^{230}Th/^{232}Th$ atomic ratio of $4.4 \pm 2.2 \times 10^{-6}$ was used to correct for the initial ^{230}Th. U–Th isotopic and concentration data, the decay constants and the calculated ages are listed in Table 1 with 2σ error.

In total, 408 powdered subsamples were drilled by using a handheld carbide dental drill at intervals of 1 mm along the central growth axes of this stalagmite for stable isotope analysis. The stable oxygen and carbon isotope compositions were measured using an Isoprime100 gas source stable isotope ratio mass spectrometer equipped with a MultiPrep system at the Institute of Earth Environment, Chinese Academy of Sciences. The international standard NBS19 and the inter-laboratory standard TB1 were run for every 10 samples and arbitrarily selected duplicate measurements were conducted every 10 to 20 samples, respectively, to check for homogeneity and reproducibility. The $\delta^{18}O$ values reported here are relative to the Vienna PeeDee Belemnite (VPDB) standard. The results of standards (i.e. NBS 19 and TB1) show that the precisions of the $\delta^{18}O$ and $\delta^{13}C$ analyses are better than 0.15 and 0.12‰ (2σ), respectively.

3. Results

3.1. Chronology

The dating results show that the concentration of uranium in stalagmite SD1 ranges from 129.9 ppb to 912.2 ppb and the concentration of thorium ranges from 1865 ppt to 36387 ppt (Table 1). Within the 2σ dating error which are typically less than 1% (except one date with ~2% error), all dates are in stratigraphic order. By

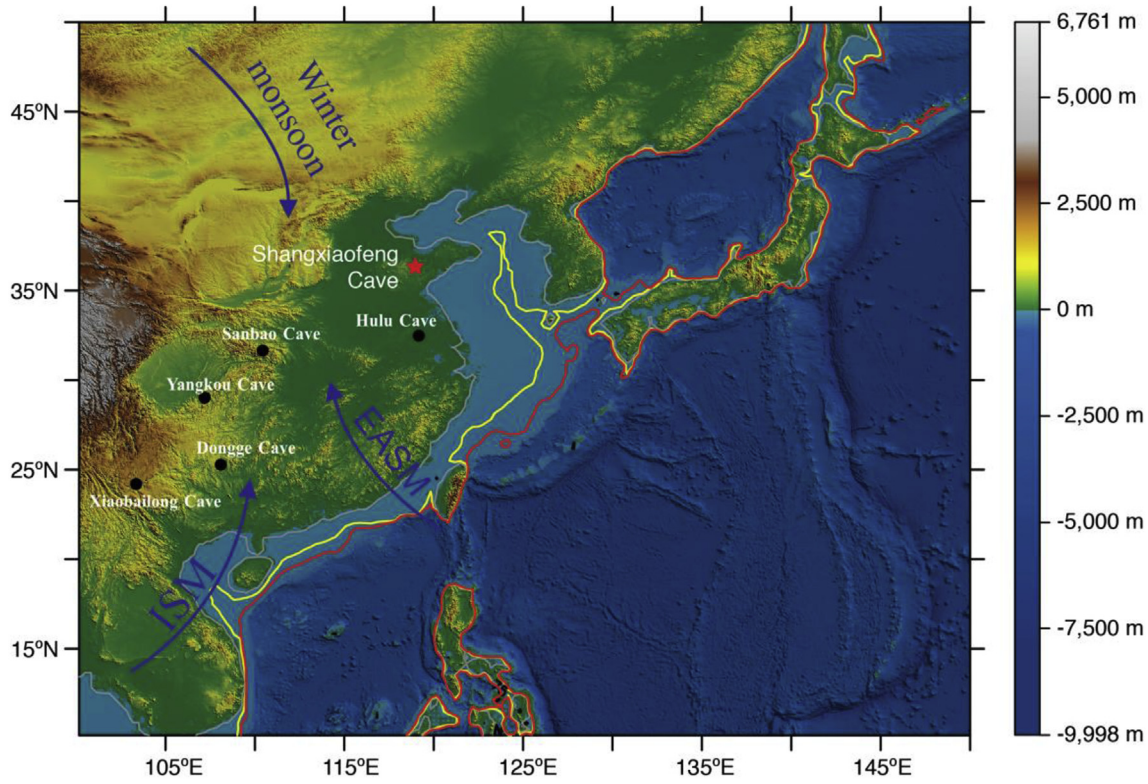

Fig. 1. Location of Shangxiaofeng Cave and other caves in topographic map: Shangxiaofeng Cave, red star; Hulu Cave, Sanbao Cave, Yangkou Cave and Xiaobailong Cave, black circles. GTOPO30 data distributed by U.S. Geological Survey's EROS (Earth Resources Observation and Science; http://eros.usgs.gov/#/Find_Data/Products_and_Data_Available/gtopo30_info) Data Center were used to plot topographic map. The yellow and red contour lines show the coastlines of sea level low-stands of −75 m and −120 m, respectively. The dark blue arrows stand for East Asian summer monsoon (EASM), Indian summer monsoon (ISM) and Asian winter monsoon, respectively. (For interpretation of the references to color in this figure legend, the reader is referred to the Web version of this article.)

using a probabilistic Monte Carlo approach method (Scholz and Hoffmann, 2011), we established the chronology for SD1 by using the StalAge application. A linear interpolated chronology was also created to compare with the StalAge chronology. The age-depth relationships obtained with these two methods are shown in Fig. 3A. Within dating errors, these two chronologies fit each other very well, indicating the reliability of our chronology. The resulting age model spans the interval from 138 ka to 125.8 ka BP, with a mean associated uncertainty of 780 years. Here we calculated growth rates of SD1 by using the linear interpolation, since the algorithm used by the StalAge application may generate unreal spark of growth rate increase. The results show that the growth rates vary from 12.9 μm/year to 125.6 μm/year (Fig. 3B).

3.2. The $\delta^{18}O$ and $\delta^{13}C$ record

The mean temporal resolution of our record is 30 years. The highest and lowest resolutions are 3 and 65 years respectively, indicating large changes in the growth rate. As shown in Fig. 4, the $\delta^{18}O$ values of SD1 vary between −4.5‰ and −10.5‰ with a mean value of −7.7‰ from 138 ka to 125.8 ka BP. To facilitate the discussion on the monsoon variation during different intervals, we used the ramp function regression (Mudelsee, 2000) to identify the change points of SD1 records. Three ramps were fitted, with the oldest transition corresponding to strong increasing of $\delta^{18}O$, and other two corresponding to weak decreasing of $\delta^{18}O$ (Fig. 4). Considering two weak decreasing of $\delta^{18}O$ occurred in succession during a short period and bear the similar structure with the speleothem records from Sanbao Cave (e.g., SB 25, Fig. 1 in Cheng et al., 2009), we merged these two transitions as one and divided the penultimate deglaciation $\delta^{18}O$ record into three main periods, i.e., 138.0–135.1 ka BP, 135.1–128.1 ka BP and 128.1–125.8 ka BP, respectively, During the first period, i.e., 138.0–135.1 ka BP, the $\delta^{18}O$ value largely fluctuated around the mean value of −7.9‰, except for a short excursion of enriched $\delta^{18}O$ from 136.4-135.7 ka BP. Then, the speleothem $\delta^{18}O$ changed to less negative and oscillated around −6.9‰ from 135.1-128.1 ka BP. It is worth noting that several enriched $\delta^{18}O$ excursions, i.e., ca. 134.5, 132.8, 128.3 ka BP, are prominent during this period, indicating abrupt climate changes. During the last period, from 128.1 to 125.8 ka BP, the $\delta^{18}O$ values increased slightly with the mean value of −8.6‰.

The $\delta^{13}C$ values varied between −5.0‰ and −12.2‰, with a long-term decreasing trend superimposed by several millennial to centennial scales fluctuations during the growth period of the stalagmite from 138.0-125.8 ka BP. Most of the millennial to centennial scales enrichments of $\delta^{13}C$ are well correlated with the increases of $\delta^{18}O$, i.e., 136, 134.5, 132.8 and 128.3 ka BP (Fig. 4), implying the contemporaneous responses of $\delta^{13}C$ to these events.

3.3. Test of equilibrium deposition

Multiple factors, including drip water $\delta^{18}O$ (amount weighted isotopic composition of meteoric precipitation), cave temperature (which is usually dominated by surface temperature), and physical processes of kinetic loss of CO_2 and possibly evaporation of water during calcite deposition, affect the speleothem stable isotope compositions. Only when deposition occurs under isotope equilibrium conditions, the speleothem $\delta^{18}O$ value can be simply ascribed to drip water $\delta^{18}O$ and cave temperature (Hendy, 1971). It is requisite to test if the isotope equilibrium conditions were

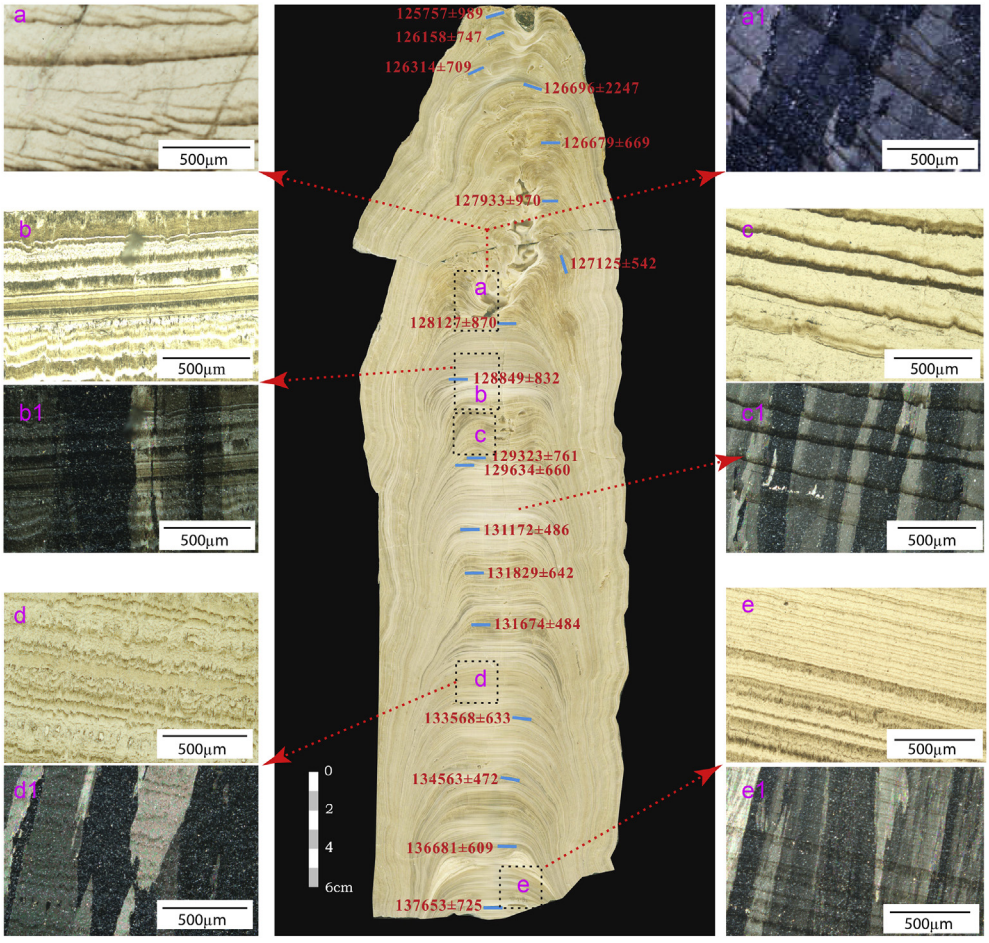

Fig. 2. The halved section and photographs of petrographic thin sections of stalagmite SD1 from Shangxiaofeng Cave. The blue bars indicate positions of U–Th dating samples, the red numbers show the ages of these samples, and the black dashed line rectangles indicate the positions of thin sections. Thin section photographs of stalagmite: a, b, c, d, e: polarized light; a1, b1, c1, d1, e1: cross-polarized light. (For interpretation of the references to color in this figure legend, the reader is referred to the Web version of this article.)

Table 1
^{230}Th dating results. The error is 2σ error.

Sample Number	Depth (mm)	^{238}U (ppb)		^{232}Th (ppt)		^{230}Th/ ^{232}Th (atomic ×10^{-6})		δ^{234}U[a] (measured)		^{230}Th/ ^{238}U (activity)		^{230}Th Age (yr) (uncorrected)		^{230} Th Age (yr) (corrected)	δ^{234}UInitial[b] (corrected)
SD-1-A1	**6**	141.5	±0.2	7503	±150	382	±8	680.2	±2.4	1.2296	±0.0042	126609	±824	**125757 ± 989**	970 ± 4
SD1-18-1	**18**	129.9	±0.2	4961	±100	521	±11	652.1	±2.1	1.2082	±0.0030	126802	±629	**126158 ± 747**	931 ± 4
SD1-28-1	**28**	145.8	±0.1	7308	±146	404	±8	676.2	±1.6	1.2293	±0.0024	127125	±478	**126314 ± 709**	966 ± 3
SD1-D1	**43**	182.4	±0.3	36387	±729	101	±2	644.2	±2.4	1.2183	±0.0026	129822	±609	**126696 ± 2247**	921 ± 7
SD1-69	**69**	177.8	±0.2	6923	±139	502	±10	618.3	±2.1	1.1842	±0.0022	127349	±519	**126679 ± 669**	884 ± 3
SD1-E1	**96**	185.1	±0.4	10458	±210	345	±7	605.0	±3.2	1.1817	±0.0030	128883	±750	**127933 ± 970**	868 ± 5
SD1-125	**125**	181.3	±0.2	5986	±120	596	±12	627.7	±1.7	1.1936	±0.0017	127699	±408	**127125 ± 542**	899 ± 3
SD1-E	**161**	170.3	±0.1	10264	±206	327	±7	619.1	±1.6	1.1943	±0.0028	129127	±571	**128127 ± 870**	889 ± 3
SD1-F1	**184**	267.2	±0.5	11982	±240	434	±9	599.5	±2.6	1.1810	±0.0028	129619	±673	**128849 ± 832**	863 ± 4
SD1-G1	**216**	369.2	±0.8	2606	±52	2794	±56	619.0	±3.1	1.1962	±0.0031	129499	±758	**129323 ± 761**	892 ± 5
SD1-220	**220**	322.2	±0.3	15443	±309	406	±8	594.6	±1.6	1.1814	±0.0015	130454	±392	**129634 ± 660**	857 ± 3
SD1-G	**245**	400.2	±0.4	8202	±164	956	±19	596.0	±1.6	1.1882	±0.0018	131560	±432	**131172 ± 486**	863 ± 3
SD1-H1	**264**	496.4	±0.9	2846	±57	3387	±68	580.6	±1.9	1.1778	±0.0028	131987	±639	**131829 ± 642**	842 ± 3
SD1-H	**285**	573.4	±0.6	4271	±86	2651	±53	605.8	±1.8	1.1978	±0.0019	131856	±477	**131674 ± 484**	879 ± 3
SD1-I1	**324**	682.4	±1.1	13840	±277	1033	±21	681.2	±2.1	1.2707	±0.0027	133931	±599	**133568 ± 633**	993 ± 4
SD1-I	**351**	680.0	±0.6	9011	±180	1662	±33	753.5	±1.7	1.3355	±0.0021	134814	±454	**134563 ± 472**	1102 ± 3
SD1-J	**379**	717.3	±1.1	1865	±37	7303	±147	521.4	±1.7	1.1519	±0.0024	136791	±608	**136681 ± 609**	767 ± 3
SD-1-A2	**405**	912.2	±1.6	10417	±209	1658	±33	511.1	±1.9	1.1483	±0.0028	137909	±714	**137652 ± 725**	754 ± 3

U decay constants: $\lambda_{238} = 1.55125 \times 10^{-10}$ (Jaffey et al., 1971) and $\lambda_{234} = 2.82206 \times 10^{-6}$ (Cheng et al., 2013). Th decay constant: $\lambda_{230} = 9.1705 \times 10^{-6}$ (Cheng et al., 2013). Corrected ^{230}Th ages assume the initial ^{230}Th/^{232}Th atomic ratio of $4.4 \pm 2.2 \times 10^{-6}$. Those are the values for a material at secular equilibrium, with the bulk earth ^{232}Th/^{238}U value of 3.8. The errors are arbitrarily assumed to be 50%.

***B.P. stands for "Before Present" where the "Present" is defined as the year 1950 A.D.

[a] $\delta\,^{234}U = ([^{234}U/^{238}U]_{activity} - 1) \times 1000$.

[b] $\delta\,^{234}U_{initial}$ was calculated based on ^{230}Th age (T), i.e., $\delta\,^{234}U_{initial} = \delta\,^{234}U_{measured} \times e^{\lambda 234 \times T}$.

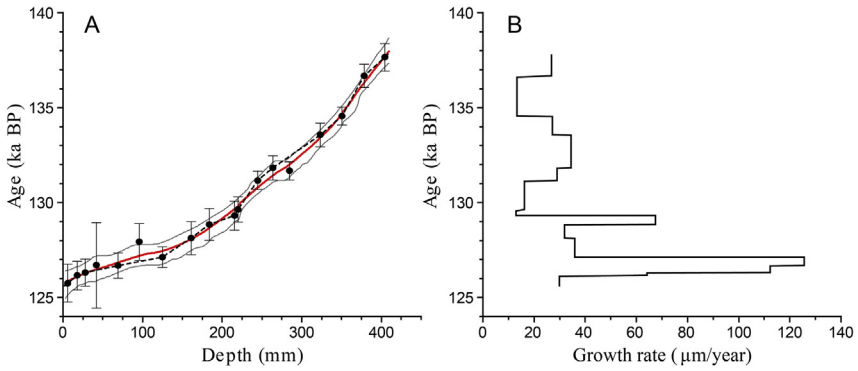

Fig. 3. Age model and calculated growth rate of stalagmite SD1. ^{230}Th dates are shown with 2σ uncertainties. (A) Age model was built by StalAge (red line) (Scholz and Hoffmann, 2011) and linear interpolation method (black dash line). The grey lines denote the upper and lower 95%-confidence limits. (B) The calculated growth rate of the stalagmite SD1 by using the linear interpolation. (For interpretation of the references to color in this figure legend, the reader is referred to the Web version of this article.)

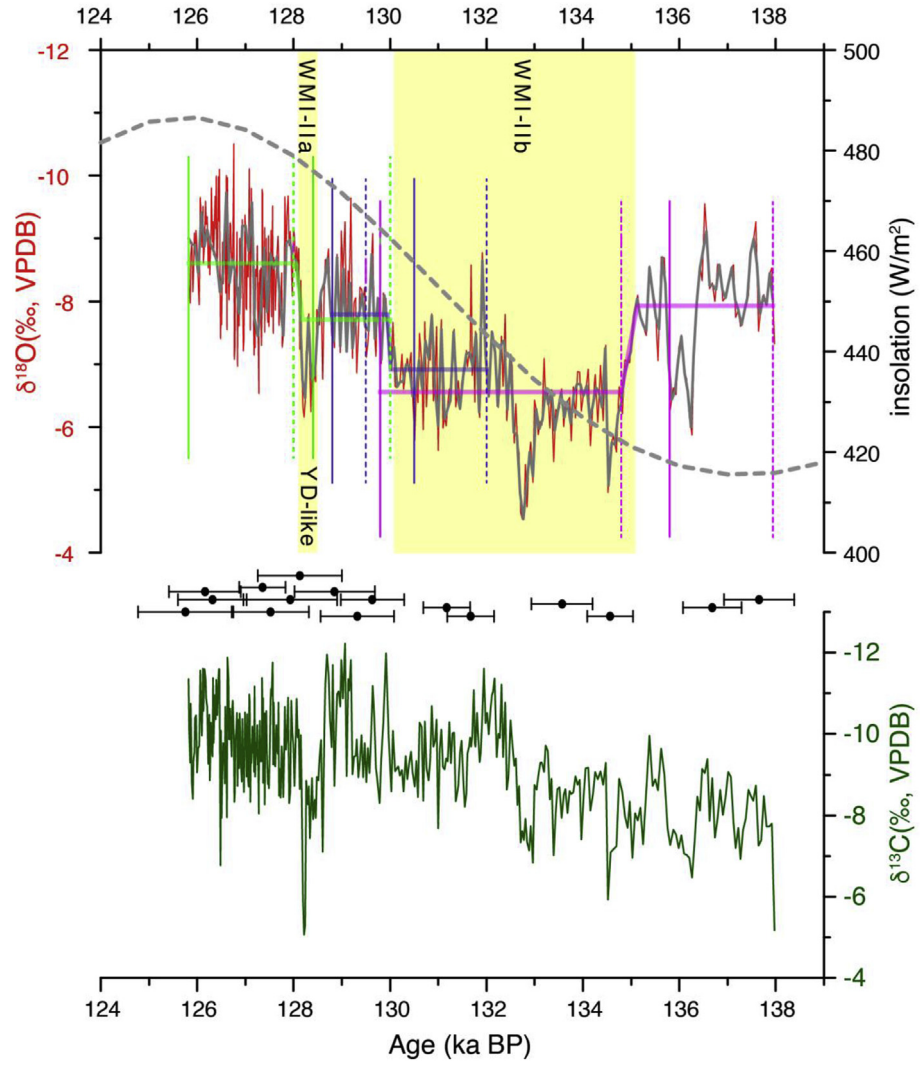

Fig. 4. The δ^{18}O (red line) and δ^{13}C (dark green line) time series of stalagmite SD1, and the mean insolation of June, July and August at 65°N (grey dash line). Yellow bars indicate WMI-IIa (YD-like event) and WMI-IIb. The ^{230}Th dates with uncertainties (±2σ) are shown as well. Three-fold Ramp function fits (light green, blue and magenta heavy line) to 65-year evenly spaced SD1 δ^{18}O time series (grey line) are also shown. Grid boundaries for t1-searches (solid vertical lines, those for young part border on t-axis) and t2-searches (dash vertical lines). Three portions are color denoted by green, blue and magenta, respectively. (For interpretation of the references to color in this figure legend, the reader is referred to the Web version of this article.)

reached during the calcite deposition, before using speleothem $\delta^{18}O$ to infer past changes in cave temperature and the isotopic composition of drip water. Following the traditional 'Hendy Test' (Hendy and Wilson, 1968), we drilled 25 sub-samples from five layers and inspected the variations of the $\delta^{18}O$ values. Indistinguishable variations in $\delta^{18}O$ are observed on same layer and there is no obvious progressively increase from central growth axis to outer edges (Fig. 5). Replication is an effective test for the fidelity of speleothem isotope time series as paleoclimate reconstructions (Dorale et al., 1998; Dorale and Liu, 2009; Wang et al., 2001). While it cannot strictly be ruled out that kinetic fractionation affects multiple replicating records equally (which would thus pass the replication test), the likelihood of kinetic fractionation is lower in well-replicating systems. Taking the quoted dating errors and temporal resolution differences into consideration, the $\delta^{18}O$ time series of SD-1 show some similarities to speleothem $\delta^{18}O$ records from Dongge, Hulu, Sanbao and Yangkou caves in segmented change pattern (Kelly et al., 2006; Cheng et al., 2006, 2009; Wang et al., 2008; Li et al., 2014) during the contemporaneous growth interval of 138-125.8 ka BP (as shown in Fig. 6). Recently, a few researchers suggested that examining the petrography could address the occurrence of the speleothem deposition close to isotopic equilibrium, and that columnar fabrics (except open columnar) are indicative of the constant degree of saturation and most likely quasi-equilibrium condition (Frisia and Borsato, 2010). We retrieved five thin-sections from different depths from SD1 stalagmite (Fig. 2). Microscopic observations of these five thin-sections indicate that the columnar is the most common fabric type in the studied stalagmite (Fig. 2), providing an independent evidence of quasi-equilibrium deposition. Therefore, it is most likely that stalagmite SD1 was formed under isotope equilibrium conditions and its $\delta^{18}O$ signal can be considered primarily of climatic origin and dictated by changes in the $\delta^{18}O$ in precipitation and cave temperature without significant kinetic fractionation (Hendy, 1971).

3.4. The interpretation of calcite $\delta^{18}O$

Under isotopic equilibrium conditions, both $\delta^{18}O$ of drip water and cave temperature jointly control the speleothem $\delta^{18}O$ (Hendy, 1971). According to the experimental studies (O'Neil et al., 1969; O'Neil, 1986) and theoretical calculations (O'Neil, 1986), the temperature dependent fractionation between the calcite and water is about −0.23‰/°C (Kim and O'Neil, 1997) at 15 °C, which means that when temperature increase of 1 °C, the calcite $\delta^{18}O$ decrease of 0.23‰. There were about ~6–8 °C temperature differences between last glacial maximum (LGM) and the Holocene Optimum (An et al., 1990; Yu et al., 2003) in northern China. Assuming the temperature changes from MIS 6 (glacial) to MIS 5e (interglacial) similar to that of the LGM-to-Holocene changes, it would account for ~1.5–2.0‰ of calcite $\delta^{18}O$ changes at our study site. This temperature-dependent calcite $\delta^{18}O$ changes would be even smaller (~1.1–1.4‰), provided we use the new empirical relationship for cave-specific water–calcite oxygen isotope fractionation, i.e., −0.177‰/°C (Tremaine et al., 2011). The speleothem calcite $\delta^{18}O$ record from Shangxiaofeng Cave shows a change of ca.~6.0‰ over the growth period from 138-125.8 ka BP, with lower $\delta^{18}O$ values during the high-temperature interglacial and higher $\delta^{18}O$ values during the low-temperature glacial. Thus, while the influence of temperature changes on the speleothem $\delta^{18}O$ on glacial-interglacial time-scale is not negligible, the variation of our stalagmite $\delta^{18}O$ values are mainly controlled by the $\delta^{18}O$ values of drip water, i.e., by variations in the oxygen isotope composition of rainfall over the cave.

In Asian monsoon regions, multiple factors have been proposed to interpret changes in the $\delta^{18}O$ of drip water, i.e., $\delta^{18}O$ of precipitation, such as changes in summer: winter precipitation ratio (Wang et al., 2001), changes in the fraction of water vapor rained out between tropical sources and the cave (Yuan et al., 2004), changes in the fraction of low $\delta^{18}O$ monsoon rainfall in annual totals (Cheng et al., 2009), and changes in moisture sources (Cai et al., 2001; Tan, 2014). It has been also suggested that the precipitation $\delta^{18}O$ at East Asia summer monsoon regions mainly reflect the changes in the $\delta^{18}O$ of atmospheric vapor in the upstream source regions over the Indian Ocean and Indian Monsoon region (Maher, 2008; Liu et al., 2014). As pointed out by Cheng et al. (2016), this interpretation is similar to the explanation of changes in the fraction of water vapor rained out between tropical sources and the cave, since the atmospheric vapor in upstream source regions also determined by the "rain-out" effect from the tropical source oceans.

Here, we largely follow the explanation by Cheng et al. (2016), and use the terms 'strong monsoon' and 'weak monsoon' to refer to low and high speleothem $\delta^{18}O$, respectively. It is worth noting that changes in circulation and moisture sources (Hoffmann and Heimann, 1997; Cai et al., 2015), and changes in ice volume also have significant influences on the precipitation $\delta^{18}O$ in our study region during the penultimate deglaciation. We will discuss their influences in detail later.

3.5. Climate change recorded in the SD1 stalagmite and comparison with other records

Our high-resolution $\delta^{18}O$ record covers the latest part of the interval that post-dates the penultimate glacial maximum, the

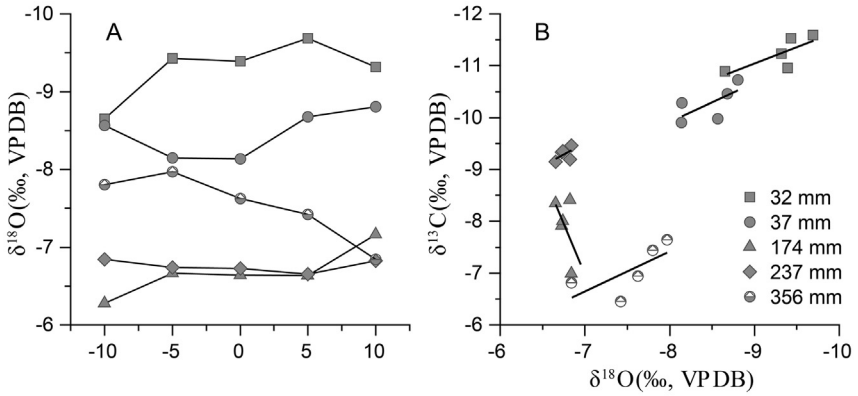

Fig. 5. Traditional Hendy test on five different layers. (A) $\delta^{18}O$ of individual laminae; (B) $\delta^{13}C$–$\delta^{18}O$ correlations along the five individual laminae.

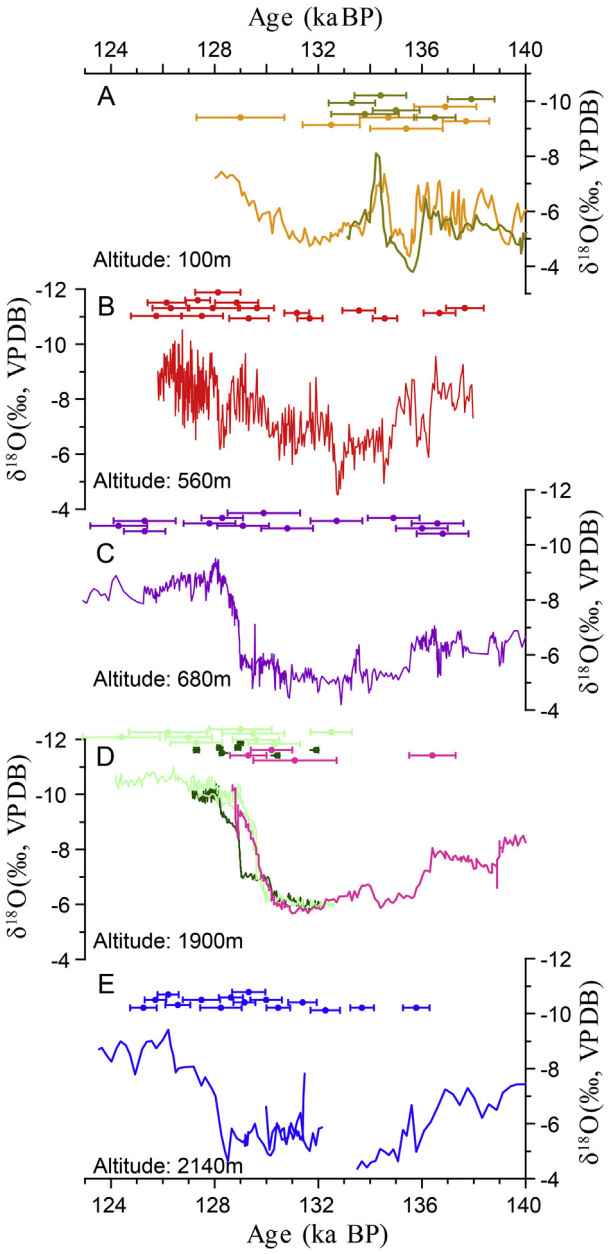

Fig. 6. The comparison of oxygen isotope records from (A) Hulu Cave (Cheng et al., 2006); (B) Shangxiaofeng Cave (this study); (C) Dongge Cave (Kelly et al., 2006); (D) Sanbao Cave (Wang et al., 2008; Cheng et al., 2009); (E) Yangkou Cave (Li et al., 2014). The ^{230}Th dates with uncertainties (±2σ) and the altitude information are shown in each plot.

penultimate deglaciation and the first part of Last Interglacial (Kelly et al., 2006; Wang et al., 2008; Cheng et al., 2009; Li et al., 2014) and provides unprecedented insights into penultimate deglacial monsoon variabilities on millennial-to-centennial scales. During the latest part of the interval that post-dates the penultimate glacial maximum, i.e., from 138.0 to 135.1 ka BP in our record, the $\delta^{18}O$ values are relatively depleted and variable, with an average of −7.9‰, likely indicating a moderate Asian summer monsoon. However, the summer monsoon intensity might be different from that indicated by the similar speleothem $\delta^{18}O$ values during the interglacial period, due to the changes in the distance to the coastline, fraction of the recycled water, and potential changes in the moisture sources associated with the circulations, and other factors (Cai et al., 2010). This episode is followed by an abrupt increase of $\delta^{18}O$ value that persisted until 128.1 ka BP, indicating a period of weak Asian summer monsoon during the deglaciation, namely, the "Weak Monsoon Interval (WMI)" proposed by Cheng et al. (2006, 2009). In addition to the general similarity to the WMI-II in other Chinese speleothem records from Hulu, Dongge, Sanbao and Yangkou caves (Cheng et al., 2006, 2009; Kelly et al., 2006; Wang et al., 2008; Li et al., 2014), the high-resolution sampling of our record reveals hitherto undocumented details, showing that this Weak Monsoon Interval comprise WMI-IIa from 128.5 to 128.1 ka BP and WMI-IIb from 135.1 to 130.1 ka BP, and it punctuated by a brief strengthening of the Asian summer monsoon from 130.1 to 128.5 ka BP. Thereafter, the depleted $\delta^{18}O$ values show a strengthened summer monsoon with slight monsoon strengthening and then weakening trend to 125.8 ka BP during the Last Interglacial.

As demonstrated by this study and previous studies on much longer time series (Wang et al., 2008; Cai et al., 2015; Cheng et al., 2016), changes in the Chinese speleothem $\delta^{18}O$ co-vary with the northern Hemisphere summer insolation changes. The co-variations between Chinese speleothem $\delta^{18}O$ record and northern hemisphere summer insolation give substance to the hypothesis that the Asian summer monsoons is driven by changes in Northern Hemisphere summer insolation on orbital time scales.

A closer look at the highly resolved records, however, reveals that insolation changes lead speleothem $\delta^{18}O$, and that monsoon variations are much more abrupt than insolation changes at the termination. Millennial-to centennial-scale fluctuations, which were superimposed on the long-term trend of Asian summer monsoon on orbital time-scale, are clearly observed during the deglaciations. For example, the $\delta^{18}O$ value abruptly increased about 3.1‰ at ~135.1 ka BP, coincided with the onsets of WMI-II, and the period with enriched $\delta^{18}O$ values from 135.1 to 130.1 ka BP and from 128.5 to 128.1 ka BP are synchronous with the WMI-II observed in other Chinese speleothem records. Furthermore, the abrupt shifts of the speleothem $\delta^{18}O$ centered at 134.5 ka, 132.8 ka and 131ka, align well with the Ice Rafted Detritus events 11 (Heinrich Events 11) complex identified from the North Atlantic marine sediments, i.e., ice rafted events recorded in MD01-2444 and ODP984, benthic $\delta^{18}O$ in ODP 983 and Uk'37 SST record in MD01-2444 (Fig. 7A, B, D, E, Channell et al., 1997; Mokeddem et al., 2014; Marino et al., 2015; Tzedakis et al., 2018).

These monsoon weakening deviations largely align with the periods of freshwater-induced weakening of the overturning circulation that resulted in North Atlantic surface water cooling (Broecker et al., 1985; Heinrich, 1988; McManus et al., 2004; Denton et al., 2010) and large-scale atmospheric perturbation, including southward shift of the Intertropical Convergence Zone (ITCZ) (Cheng et al., 2009; Denton et al., 2010). These coincidences further substantiate the teleconnection between North Atlantic climate changes and variations of Asian summer monsoons.

Carbon isotope composition reflects variations in vegetation's type and density, and in soil microbial activities (Genty et al., 2003; McDermott, 2004). Stalagmite $\delta^{13}C$ values of −14‰ to −6‰ are typical values for C3 plants and values of −6‰ to +2‰ for C4 plants above the cave (Dreybrodt, 1980; Baker et al., 1997; McDermott, 2004). In general, when the climate is warm and wet, the overlying ecosystem largely enriched in C3 plants, more density vegetation and dynamic soil microbial activities, and vice versa (Genty et al., 2010; Hartmann et al., 2013).

The $\delta^{13}C$ values of stalagmite SD1 range from −12.2‰ to −5.0‰, with most values less than −6.0‰, indicating the domination of C3 plants at the study site. The long-term decreasing trend of the $\delta^{13}C$ values largely suggests the increasing vegetation cover and intensifying soil microbial activities, and possibly shorting residence

time of the seeping water within the cave systems, implying the strengthening Asian summer monsoon during the penultimate deglaciation. Moreover, several fluctuations of increased $\delta^{13}C$ on millennial to centennial scales also exist during the period from 138 ka to 125.8 ka BP. These abrupt fluctuations of $\delta^{13}C$ values are aligned with the oscillations of $\delta^{18}O$ values, i.e., ca 134.5 ka, 132.8 ka and 128.3 ka BP, hinting at the responses of vegetation type/cover and soil microbial activities to the climate changes, i.e., the cold-dry climate conditions linked to the North Atlantic ice-rafted detritus events worst the local vegetation and soil microbial activities.

As a whole, our records provide further evidence from the northern China that not only northern Hemisphere insolation (on orbital scales), but also North Atlantic climate changes (on millennial-centennial scales) (i.e. Heinrich Events) are important in affecting the Asian summer monsoon variations (Cai et al., 2006; Dykoski et al., 2005; Kelly et al., 2006; Wang et al., 2008; Cheng et al., 2009).

3.6. A YD like event at the end of the Termination-II?

A close inspection reveals the presence of two Weak Monsoon Intervals (WMIs) and one interstadial during termination II. As shown in Fig. 4, WMI-IIa occurred between128.5 and 128.1 ka BP and lasted approximate 400 years. WMI-IIb happened between 135.1 and 130.1 ka BP and lasted about 5000 years. Sandwiched between these two WMIs, there is an episode of a moderate monsoon strengthening with a duration of 1600 years (130.1−~128.5 ka BP). The two excursions of WMI-IIa and WMI-IIb observed in our study differ from the speleothem records from Dongge Cave, southern China where only one weak monsoon interval was found in the speleothem $\delta^{18}O$ records (Yuan et al., 2004; Kelly et al., 2006). For the Sanbao Cave, there are three stalagmites spanning the period from 132.2 to 128.7 ka BP. We noticed that the $\delta^{18}O$ record of stalagmite SB11 also has an abrupt shift at ~128.9 ka BP (Fig. 7F), while other two stalagmites in the same cave do not have such event (Wang et al., 2008). Although this abrupt shift lasts a short time period of ~100 years, it likely indicates that there indeed exists a weak monsoon event. The absence of WMI-IIa event in the Dongge and Yangkou cave records is most likely not related to a spatial variability but to the relatively low resolution of these records.

Indeed, similar event correlated to the WMI-IIa within Termination II has also been identified in the speleothem records from Europe. Regattieri et al. (2014) reported a speleothem record from Tana che Urla Cave (TCU) in central Italy. The TCU $\delta^{18}O$ record shows significant multi-centennial variability between approximately 131.0 ka and 121.4 ka BP. One short prominent event centered at ca. 129.6 ± 1.0 ka, with elevated speleothem $\delta^{18}O$, indicates reduced precipitation during this period (Fig. 7G). Considering the chronology uncertainties of 800 years in our record, this event is likely synchronous with the WMI-IIa event in our record, implying that both the SD1 and TCU cave records respond to change in North Atlantic climate that captured in several marine records that indicate an abrupt cold event (anomaly event) during Termination II (McManus et al., 1994; Oppo et al., 1997; Sarnthein and Tiedemann, 1990; Bauch et al., 2012; Risebrobakken et al., 2006; Lukashina and Bashirova, 2015; Lototskaya and Ganssen, 1999; Goñi et al., 1999; Cortese and Abelmann, 2002). However, due to the uncertainty in the chronology and different temporal resolution, this brief excursion during Termination II are registered, in part, asynchronously.

The Younger Dryas event during the last deglaciation has been found to be an abrupt event with hemispheric influences. It is broadly ascribed to enhanced freshwater input into the North Atlantic Ocean that resulted in a weakening of North Atlantic overturning circulation accompanied by the spread of winter sea

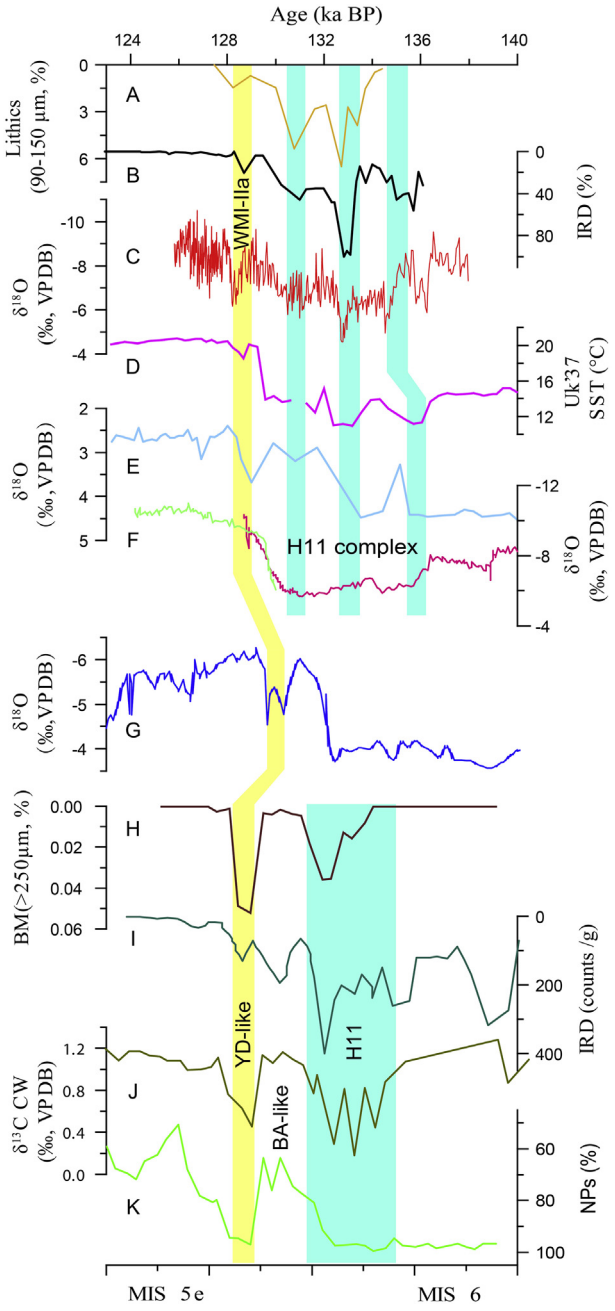

Fig. 7. Comparison of various records during the penultimate deglaciation. (A) IRD record from North Atlantic sediment (MD01-2444). It was digitized from Marino et al. (2015). Its chronology modified by Marino et al. (2015) due to the Sample spacing (1σ) uncertainties and dating uncertainties in different sediments (Skinner and Shackleton, 2006; Marino et al., 2015); (B) IRD record from ODP984 (Mokeddem et al., 2014); (C) Shangxiaofeng Cave $\delta^{18}O$ (this study); (D) Alkenone $^{Uk'}37$ sea surface temperature record from MD01-2444 (Tzedakis et al., 2018); (E) A benthic $\delta^{18}O$ data from ODP983 (Channell et al., 1997); (F) Sanbao Cave records (Wang et al., 2008); (G) Tana Che Urla Cave record (Apuan Alps, central Italy) (Regattieri et al., 2014); (H)-(K) stands for the records from PS1243 at the eastern Polar Gyre near the Arctic front of the southern Nordic seas (Bauch et al., 2012), all the data was digitized by Getdata. (H) Relative abundance of the large sized, subtropical planktic foraminifer *Beella megastoma* (BM); (I) Number of iceberg-rafted debris per gram sediment and >250 μm; (J) Bottom water $\delta^{13}C$ of the species *C. wuellerstorfi* (CW); (K) NPs% from PS1243 indicates the North Atlantic sea surface temperature variation. The vertical yellow bar indicates the YD-like event in various sediments. The IRD events corresponded to H11 are indicated by vertical cyan bars. Note: Bottom picture's chronology are based on Marine Isotope Stage. (For interpretation of the references to color in this figure legend, the reader is referred to the Web version of this article.)

ice and cold ocean temperatures. Around the termination II, ice rafted event corresponding to the WMI-IIa event is evident in many of ocean sediments from North Atlantic (Fig. 7A, B, 7I) (Bauch et al., 2012; Lukashina and Bashirova, 2015; Risebrobakken et al., 2006; Mokeddem et al., 2014; Skinner and Shackleton, 2006; Marino et al., 2015), while the prominent Heinrich event 11 correlated with the WMI-IIb. Coincidentally, North Atlantic benthic $\delta^{18}O$ shows a positive shift during Termination II, although the amplitude is small, and the duration is short for this shift (Fig. 7E). This observation lends credence to the notion that the melting of ice sheet. Furthermore, North hemisphere sea surface temperature (SST) records (Fig. 7D, H, 7K) which are indicated by alkenones Uk'37 record and relative abundance of planktonic foraminifers also has similar structure during Termination II (Bauch et al., 2012; Tzedakis et al., 2018). A decreasing trend likely caused by IRD event, shows a relatively low sea surface temperature likely coincided with WMI-IIa event and deep-dwelling species co-occurred with strong depletions in benthic $\delta^{13}C$ during deglacial cold events as shown by bottom water $\delta^{13}C$ (Fig. 7J) during this short interval. All these lines of evidence indicate the occurrence of WMI-IIa event during the Termination II, although it is not as pronounced as Younger Dryas during Termination I.

The model simulation conducted by Sima et al. (2004), which was forced with the ice-volume history generated by a one-dimensional coupled ice-sheet-bedrock model, predicts Younger-Dryas-type cooling events for each major glacial termination, implying that the Younger Dryas does not appear to be a one-time event. In fact, as exemplified by the Chinese speleothem $\delta^{18}O$ records spanning the past 640,000 years, Younger-Dryas-type event also occurred at Termination III and Termination VII (Cheng et al., 2009, 2016). We therefore, suggest that Younger-Dryas-type events are an intrinsic feature of climate change during the termination of ice age, and our WMI-IIa might be a Younger-Dryas-type event during the Termination II.

It is worth noting that a recent study from south Europe proposed that the excursion at ca. 128.5 ka BP might be the first climate events during the Last Interglacial, which is corresponded to a North Atlantic cold excursion and ice rafted event (i.e., C28, in Tzedakis et al., 2018). The further study on the stalagmite sample from Tana che Urla Cave (TCU) in central Italy also aligned the event between 130.7 and 129.6 ka with the part of Heinrich event 11 complex during the penultimate deglaciation (Regattieri et al., 2016). These studies called into question the existence of a YD-like event during the penultimate deglaciation and complicated our cognizance of YD-like events during the Terminations. However, for the reason that climatic responses are diverse in different regions, i.e. the timing and the duration of the penultimate deglaciation, of the Last Interglacial "acme" and the last glacial inception vary from one record to another (Govin et al., 2015; Hauselmann et al., 2015), or low sedimentary resolution is likely mask the brief Younger-Dryas-type events during other Terminations in different records, the brief Younger-Dryas-type event is hardly to be identified repeatedly as the one during the last deglaciation. More well-dated high-resolution records during the deglaciation at different regions are essential to understand the climate change during the Termination in-depth.

3.7. Sea-level changes and its impacts on the $\delta^{18}O$ of regional precipitation

Significant disparities between SD1 and Dongge, Sanbao and Yangkou $\delta^{18}O$ records exist, particularly, in terms of the glacial-interglacial $\delta^{18}O$ value difference. As depicted in Fig. 8, the dissimilarity between our $\delta^{18}O$ record and other Chinese speleothem records from southern China lies in the mean $\delta^{18}O$ value between interglacial interval from ~125.8 to ~128.1 ka BP, and glacial interval from 135.1 to 138 ka BP in our SD1 record. This difference is about ~0.7‰ in our SD1 record and corresponding differences in other records from Yangkou, Dongge and Sanbao caves are ~1.4‰,~2.2‰ and ~2.4‰, respectively (Fig. 8). Considering the ice-volume related changes in isotope composition of ocean water (~1.0‰, Shackleton, 2000), the actual differences between glacial and interglacial intervals would be smaller than those observed. However, the aforementioned disparity between our SD1 record and other Chinese speleothem records remains, since the ice-volume related mean $\delta^{18}O$ variation in ocean water affects all the cave records in the same way.

Difference in altitude is a significant factor contributing to this dissimilarity because the high elevation of the cave site may amplify the rainout processes, leading to the increased amplitude of the precipitation $\delta^{18}O$ variation (Cai et al., 2012, reference therein). However, the $\delta^{18}O$ difference between glacial and interglacial intervals in Dongge record is similar with that of Sanbao records, whereas their altitudes are very different, i.e. 680 m for Dongge Cave and 1900 m for Sanbao Cave, implying that this dissimilarity is most likely caused by other factors.

Although the temperature has minor effect on oxygen isotope composition of speleothem calcite, i.e., the temperature dependent fractionation between the calcite and water is about −0.23‰/°C (Kim and O'Neil, 1997), the decreased amplitude in temperature changes from high latitude to low latitude (Herbert et al., 2016, reference therein) suggests that temperature might be a potential

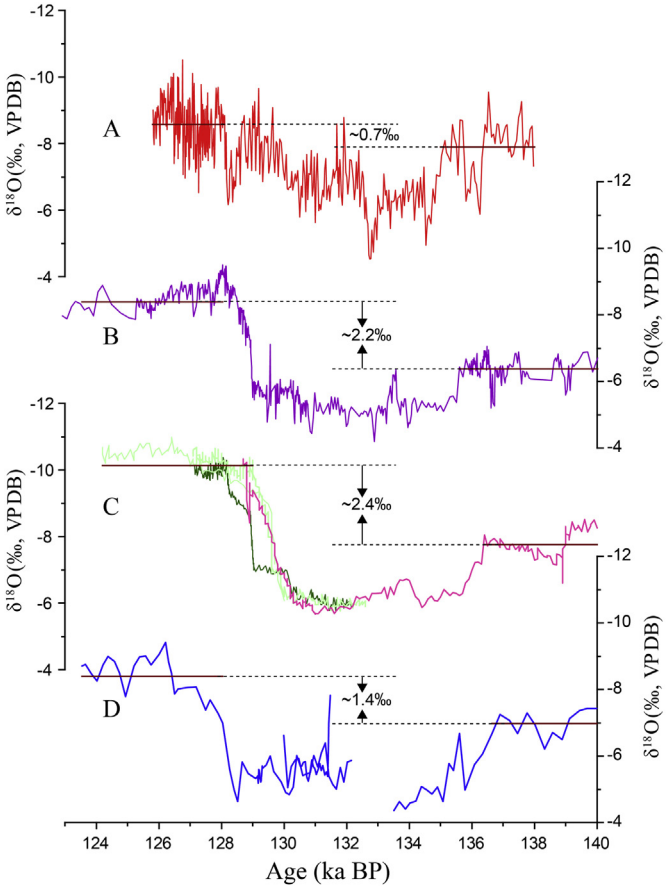

Fig. 8. The $\delta^{18}O$ difference between penultimate glacial and interglacial period of (A) Shangxiaofeng cave (this study), (B) Dongge cave (Kelly et al., 2006), (C) Sanbao cave (Wang et al., 2008; Cheng et al., 2009). (D) Yangkou Cave (Li et al., 2014). The solid lines represent the time intervals for calculating the mean $\delta^{18}O$ values.

factor contributing to the difference in amplitude between southern and northern China on glacial-interglacial time-scales. However, the amplitude of temperature change at the Shangxiaofeng Cave site in northern China may be larger than that of low latitude Asian Monsoon regions, i.e., southern China. The increased amplitude of temperature changes between glacial and interglacial could enlarge the speleothem $\delta^{18}O$ difference at our cave site. This is opposite to the observation that the speleothem calcite $\delta^{18}O$ difference between glacial and interglacial (i.e. between interglacial interval from ~125.8 to ~128.1 ka BP, and glacial period from 135.1 to 138 ka BP) at southern China record is much larger than our SD1 record in northern China (Fig. 8). Thus, temperature possibly is not a significant factor that influenced the amplitude of Chinese speleothem $\delta^{18}O$ in penultimate deglaciation period and this in some extent further infers that changes in circulation and moisture source are substantial factors to be considered.

Cai et al. (2015) have examined the glacial-interglacial differences of speleothem $\delta^{18}O$ values from East China and Southwest China. They found the speleothem calcite $\delta^{18}O$ values between marine isotope stages (MISs) 5 and 3 are large and distinct at Southwest China where Indian summer monsoon dominates and barely discernible in speleothem $\delta^{18}O$ records in Eastern China where East Asian summer monsoon prevailed. Changes in atmospheric circulations and rainfall, and particularly, the reduced evaporation over exposed continental shelf during the LGM have been proposed to contribute to the depleted precipitation $\delta^{18}O$ downstream at the cave sites in East China. We suggest that similar mechanisms could be used to interpret the disparity observed here.

Sea levels have fluctuated throughout geological times with amplitudes of hundred meters associated with melting and accumulating of continental ice-sheets on glacial-interglacial timescales during the Quaternary. Alternations of sea level highstands and lowstands resulted in the shifts of coastlines across coastal plains. Due to the broad continental shelf, the coastline shifted in East China could be ~300–1000 km during the glacial maxima of last 800 ka when sea-levels were about 120-m lower than present (Chappell and Shackleton, 1986; Spratt and Lisiecki, 2016; Medina-Elizalde, 2013; Peltier, 2004). As show in Fig. 1, the Bohai Sea and large parts of Yellow Sea would be exposed when sea-level is about 75m lower than present time and both Bohai Sea, Yellow Sea and large parts of East China Sea would be exposed when seal-level is ~120 m lower than present time, increasing the distance from our cave site to ocean from 100 km to 500 and more than 800 km, respectively. Although the coastlines at southern China were also shifted southward and increased the distance from ocean to Dongge, Sanbao and Yangkou Caves (Fig. 1), the increased distance are only from 100 to 300 km, thus much less than that at our cave site. The greatly increased distance from our cave site to ocean would likely deplete the precipitation $\delta^{18}O$, resulting in the muted contrast of precipitation $\delta^{18}O$ between glacial and interglacial periods.

Furthermore, the exposure of continental shelf can change the lower boundary conditions and potentially generate the changes in atmospheric circulation and moisture fluxes from different sources. These changes might contribute this amplitude disparity as well. Yet, it is still unclear how and to what extent the exposed continental shelf (i.e. Yellow Sea and Bohai Sea) affect the contribution of the different moisture sources to the precipitation and hence the precipitation $\delta^{18}O$ at different regions during the deglaciation. Answering this question will require high-resolution simulations with sophisticated isotope enabled climate models.

4. Conclusions

We have established a high-resolution $\delta^{18}O$ and $\delta^{13}C$ records of a stalagmite spanning the time period from 138.0-125.8 ka BP from Shangxiaofeng Cave, Shandong Province, eastern China. Our speleothem $\delta^{18}O$ record largely documents changes in precipitation $\delta^{18}O$, although the influence of the temperature variations cannot be ignored. Although the SD1 $\delta^{18}O$ record diverges from Sanbao, Dongge, Yangkou cave records in detailed pattern and amplitude (such as: YD-like), however, in segmented variation pattern, it resembles other speleothem $\delta^{18}O$ records from Sanbao, Dongge and Yangkou Caves, especially Hulu Cave, indicating significant changes of the East Asian summer monsoon intensity during the penultimate deglaciation, i.e., relatively weak, weakest and strengthened East Asian summer monsoon during the glacial, 'weak monsoon interval' and Last Interglacial periods, respectively. The similarity of our speleothem $\delta^{18}O$ record with other speleothem $\delta^{18}O$ records from southern China and the correspondence between Chinese speleothem records and North Atlantic climate changes, further demonstrate the tele-connections of the East Asian summer monsoon and North Atlantic climate changes.

Our high-resolution record allows to unravel a centennial-scale weak summer monsoon interval around the ~128.3 ka BP. This WMI-IIa (YD-like event) may be synchronous with events that have been observed in speleothem record in central Italy and in several marine records, lending supports to the existence of hemisphere-wide YD-like event during the penultimate deglaciation.

We also suggest that altitude is a non-ignorable factor affecting the amplitude of speleothem $\delta^{18}O$ between glacial and interglacial. However, more importantly, sea-level changes of more than 120 m during the deglacial do have substantial impacts on the $\delta^{18}O$ of the stalagmite by shifting the coastline and changing the distance from ocean moisture source to our cave site. Increased distance from ocean moisture source to our cave site and changed atmospheric circulations caused by the exposed continental shelf at Bohai Sea and Yellow Sea likely contributed to the muted precipitation $\delta^{18}O$ difference between glacial and interglacial period.

Acknowledgements

We thank Syee Weldeab for discussions of earlier versions of the manuscript, Ashish Sinha for improve the English writing, and two anonymous reviewers for their helpful comments and suggestions. This work was supported by the National Key Research and Development Program of China (2017YFA0603401), the Chinese Academy of Sciences (grant XDPB05) and the U.S. National Science Foundation Grant 1702816 (to R.L. Edwards and H. Cheng). We also thank J. Zhou for his help of our figures.

Appendix A. Supplementary data

Supplementary data to this article can be found online at https://doi.org/10.1016/j.quascirev.2019.02.023.

References

An, Z., Wu, X., Lu, Y., Zhang, D., Sun, X., Dong, G., 1990. A Preliminary Study on the Paleoenvironment Change of China during the Last 20,000 Years. Loess, Quaternary Geology and Global Change. Science Press, Beijing, pp. 21–26.

Anchukaitis, K.J., Buckley, B.M., Cook, E.R., Cook, B.I., D'Arrigo, R.D., Ammann, C.M., 2010. Influence of volcanic eruptions on the climate of the Asian monsoon region. Geophys. Res. Lett. 37, L22703.

Baker, A., Ito, E., Smart, P.L., McEwan, R.F., 1997. Elevated and variable values of δ13C in speleothems in a British cave system. Chem. Geol. 136, 263–270.

Bauch, H.A., Kandiano, E.S., Helmke, J.P., 2012. Contrasting ocean changes between the subpolar and polar North Atlantic during the past 135 ka. Geophys. Res. Lett. 39. L11604.

Broecker, W.S., Peteet, D.M., Rind, D., 1985. Does the ocean–atmosphere system have more than one stable mode of operation? Nature 315, 21–26.

Cai, Y., Zhang, M., Peng, Z., Lin, Y., An, Z., Zhang, Z., Cao, Y., 2001. The δ ^{18} O variation of a stalagmite from Qixing Cave, Guizhou Province and indicated climate

change during the Holocene. Chin. Sci. Bull. 46, 1904–1908.
Cai, Y., An, Z., Cheng, H., Edwards, R.L., Kelly, M.J., Liu, W., Wang, X., Shen, C.-C., 2006. High-resolution absolute-dated Indian Monsoon record between 53 and 36 ka from Xiaobailong Cave, southwestern China. Geology 34, 621–624.
Cai, Y., Tan, L., Cheng, H., An, Z., Edwards, R.L., Kelly, M.J., Kong, X., Wang, X., 2010. The variation of summer monsoon precipitation in central China since the last deglaciation. Earth Planet. Sci. Lett. 291, 21–31.
Cai, Y., Zhang, H., Cheng, H., An, Z., Lawrence Edwards, R., Wang, X., Tan, L., Liang, F., Wang, J., Kelly, M., 2012. The Holocene Indian monsoon variability over the southern Tibetan Plateau and its teleconnections. Earth Planet. Sci. Lett. 335–336, 135–144.
Cai, Y., Fung, I.Y., Edwards, R.L., An, Z., Cheng, H., Lee, J.E., Tan, L., Shen, C.-C., Wang, X., Day, J.A., Zhou, W., Kelly, M., Chiang, J., 2015. Variability of stalagmite-inferred Indian monsoon precipitation over the past 252,000 y. Proc. Natl. Acad. Sci. Unit. States Am. 112, 2954–2959.
Channell, J.E.T., Hodell, D.A., Lehman, B., 1997. Relative geomagnetic paleointensity and δ18O at ODP site 983 (Gardar Drift, north Atlantic) since 350ka. Earth Planet. Sci. Lett. 153, 103–118.
Chappell, J., Shackleton, N., 1986. Oxygen isotopes and sea level. Nature 324, 137–140.
Cheng, H., Edwards, R.L., Wang, Y., Kong, X., Ming, Y., Kelly, M.J., Wang, X., Gallup, C.D., Liu, W., 2006. A penultimate glacial monsoon record from Hulu Cave and two-phase glacial terminations. Geology 34, 217–220.
Cheng, H., Edwards, R.L., Broecker, W.S., Denton, G.H., Kong, X., Wang, Y., Zhang, R., Wang, X., 2009. Ice age terminations. Science 326, 248–252.
Cheng, H., Edwards, R.L., Shen, C.-C., Polyak, V.J., Asmerom, Y., Woodhead, J., Hellstrom, J., Wang, Y., Kong, X., Spötl, C., Wang, X., Calvin Alexander, E., 2013. Improvements in 230Th dating, 230Th and 234U half-life values, and U–Th isotopic measurements by multi-collector inductively coupled plasma mass spectrometry. Earth Planet. Sci. Lett. 371–372, 82–91.
Cheng, H., Edwards, R.L., Sinha, A., Spotl, C., Yi, L., Chen, S., Kelly, M., Kathayat, G., Wang, X., Li, X., Kong, X., Wang, Y., Ning, Y., Zhang, H., 2016. The Asian monsoon over the past 640,000 years and ice age terminations. Nature 534, 640–646.
Clemens, S., Prell, W., Murray, D., Shimmield, G., Weedon, G., 1991. Forcing mechanisms of the Indian Ocean monsoon. Nature 353, 720–725.
Clemens, S.C., Prell, W.L., Sun, Y., 2010. Orbital-scale timing and mechanisms driving Late Pleistocene Indo-Asian summer monsoons: reinterpreting cave speleothem δ18O. Paleoceanography 25. PA4207.
Cortese, G., Abelmann, A., 2002. Radiolarian-based paleotemperatures during the last 160 kyr at ODP site 1089 (southern ocean, Atlantic sector). Palaeogeogr. Palaeoclimatol. Palaeoecol. 182, 259–286.
Cosford, J., Qing, H., Eglington, B., Mattey, D., Yuan, D., Zhang, M., Cheng, H., 2008. East Asian monsoon variability since the Mid-Holocene recorded in a high-resolution, absolute-dated aragonite speleothem from eastern China. Earth Planet. Sci. Lett. 275, 296–307.
Dayem, K.E., Molnar, P., Battisti, D.S., Roe, G.H., 2010. Lessons learned from oxygen isotopes in modern precipitation applied to interpretation of speleothem records of paleoclimate from eastern Asia. Earth Planet. Sci. Lett. 295, 219–230.
Denton, G.H., Anderson, R.F., Toggweiler, J.R., Edwards, R.L., Schaefer, J.M., Putnam, A.E., 2010. The last glacial termination. Science 328, 1652–1656.
Dorale, J.A., Liu, Z., 2009. Limitations of Hendy test criteria in judging the paleoclimatic suitability of speleothems and the need for replication. J. Cave Karst Stud. 71, 73–80.
Dorale, J.A., Edwards, R.L., Ito, E., González, L.A., 1998. Climate and vegetation history of the midcontinent from 75 to 25 ka: a speleothem record from Crevice Cave, Missouri, USA. Science 282, 1871–1874.
Dreybrodt, W., 1980. Deposition of calcite from thin films of calcareous solutions and the growth of speleothems. Chem. Geol. 29, 89–105.
Dykoski, C., Edwards, R., Cheng, H., Yuan, D., Cai, Y., Zhang, M., Lin, Y., Qing, J., An, Z., Revenaugh, J., 2005. A high-resolution, absolute-dated Holocene and deglacial Asian monsoon record from Dongge Cave, China. Earth Planet. Sci. Lett. 233, 71–86.
Edwards, R.L., Chen, J.H., Wasserburg, G.J., 1987. 238U-234U-230Th-232Th systematics and the precise measurement of time over the past 500,000 years. Earth Planet. Sci. Lett. 81, 175–192.
Frisia, S., Borsato, A., 2010. Karst. Dev. Sedimentol. 61, 269–318.
Genty, D., Blamart, D., Ouahdi, R., Gilmour, M., Baker, A., Jouzel, J., Van-Exter, S., 2003. Precise dating of Dansgaard–Oeschger climate oscillations in western Europe from stalagmite data. Nature 421, 833–837.
Genty, D., Combourieu-Nebout, N., Peyron, O., Blamart, D., Wainer, K., Mansuri, F., Ghaleb, B., Isabello, L., Dormoy, I., von Grafenstein, U., Bonelli, S., Landais, A., Brauer, A., 2010. Isotopic characterization of rapid climatic events during OIS3 and OIS4 in Villars Cave stalagmites (SW-France) and correlation with Atlantic and Mediterranean pollen records. Quat. Res. 29, 2799–2820.
Goñi, M.S., Eynaud, F., Turon, J.L., Shackleton, N.J., 1999. High resolution palynological record off the Iberian margin: direct land-sea correlation for the Last Interglacial complex. Earth Planet. Sci. Lett. 171, 123–137.
Govin, A., Capron, E., Tzedakis, P.C., Verheyden, S., Ghaleb, B., Hillaire-Marcel, C., St-Onge, G., Stoner, J.S., Bassinot, F., Bazin, L., Blunier, T., Combourieu-Nebout, N., ElOuahabi, A., Genty, D., Gersonde, R., Jimenez-Amat, P., Landais, A., Martrat, B., Masson-Delmotte, V., Parrenin, F., Seidenkrantz, M.S., Veres, D., Waelbroeck, C., Zahn, R., 2015. Sequence of events from the onset to the demise of the Last Interglacial: evaluating strengths and limitations of chronologies used in climaticarchives. Quat. Sci. Rev. 129, 1–36.
Hartmann, A., Eiche, E., Neumann, T., Fohlmeister, J., Schröder-Ritzrau, A., Mangini, A., Haryono, E., 2013. Multi-proxy evidence for human-induced deforestation and cultivation from a late Holocene stalagmite from middle Java, Indonesia[J]. Chem. Geol. 357, 8–17.
Hauselmann, A.D., Fleitmann, D., Cheng, H., Tabersky, D., Günther, D., Edwards, R.L., 2015. Timing and nature of the penultimate deglaciation in a high alpine stalagmite from Switzerland. Quat. Sci. Rev. 126, 264–275.
Heinrich, H., 1988. Origin and consequences of cyclic ice rafting in the northeast Atlantic Ocean during the past 130,000 years. Quat. Res. 29, 142–152.
Hendy, C.H., 1971. The isotopic geochemistry of speleothems—I. The calculation of the effects of different modes of formation on the isotopic composition of speleothems and their applicability as palaeoclimatic indicators. Geochem. Cosmochim. Acta 35, 801–824.
Hendy, C.H., Wilson, A.T., 1968. Palaeoclimatic data from speleothems. Nature 219, 48–51.
Herbert, T.D., Lawrence, K.T., Tzanova, A., Peterson, L.C., Caballero-Gill, R., Kelly, C.S., 2016. Late Miocene global cooling and the rise of modern ecosystems. Nat. Geosci. 9, 843–847.
Hoffmann, G., Heimann, M., 1997. Water isotope modeling in the Asian monsoon region. Quat. Int. 37, 115–128.
Jaffey, A.H.K., Flynn, F., Glendenin, L.E., Bentley, W.C., Essling, A.M., 1971. Precision measurement of half-lives and specific activities of 235U and 238U. Phys. Rev. C 4, 1889–1906.
Jimenez-Amat, P., Zahn, R., 2015. Offset timing of climate oscillations during the last two glacial-interglacial transitions connected with large-scale freshwater perturbation. Paleoceanography and Paleoclimatology 30 (6), 768–788.
Kelly, M.J., Edwards, R.L., Cheng, H., Yuan, D., Cai, Y., Zhang, M., Lin, Y., An, Z., 2006. High resolution characterization of the Asian Monsoon between 146,000 and 99,000 years B.P. from Dongge Cave, China and global correlation of events surrounding Termination II. Palaeogeogr. Palaeoclimatol. Palaeoecol. 236, 20–38.
Kim, S.T., O'Neil, J.R., 1997. Equilibrium and nonequilibrium oxygen isotope effects in synthetic carbonates. Geochem. Cosmochim. Acta 61, 3461–3475.
Kutzbach, J.E., Liu, Z., 1997. Response of the African monsoon to orbital forcing and ocean feedbacks in the middle Holocene. Science 278, 440–443.
Li, T.Y., Shen, C.C., Huang, L.J., Jiang, X.Y., Yang, X.L., Mii, H.S., Lee, S.Y., Lo, L., 2014. Stalagmite-inferred variability of the Asian summer monsoon during the penultimate glacial–interglacial period. Clim. Past 10, 1211–1219.
Liu, Z., Wen, X., Brady, E.C., Otto-Bliesner, B., Yu, G., Lu, H., Cheng, H., Wang, Y., Zheng, W., Ding, Y., Edwards, R.L., Cheng, J., Liu, W., Yang, H., 2014. Chinese cave records and the east Asia summer monsoon. Quat. Sci. Rev. 83, 115–128.
Lototskaya, A., Ganssen, G.M., 1999. The structure of termination II (penultimate deglaciation and Eemian) in the north Atlantic. Quat. Sci. Rev. 18, 1641–1654.
Lu, Q., Liang, F., Bi, X., Duffy, R., Zhao, Z., 2011. Effects of urbanization and industrialization on agricultural land use in Shandong Peninsula of China. Ecol. Indicat. 11, 1710–1714.
Lukashina, N.P., Bashirova, L.D., 2015. Deep water masses in the Iceland Basin during the Last Interglacial (MIS 5e): evidence from benthic foraminiferal data. Oceanologia 57, 212–221.
Maher, B.A., 2008. Holocene variability of the East Asian summer monsoon from Chinese cave records: a re-assessment. Holocene 18, 861–866.
Marino, G., Rohling, E.J., Rodriguez-Sanz, L., Grant, K.M., Heslop, D., Roberts, A.P., Stanford, J.D., Yu, J., 2015. Bipolar seesaw control on last interglacial sea level. Nature 522, 197–201.
Martrat, B., Jimenez-Amat, P., Zahn, R., Grimalt, J.O., 2014. Similarities and dissimilarities between the last two deglaciations and interglaciations in the North Atlantic region. Quat. Sci. Rev. 99, 122–134.
McDermott, F., 2004. Palaeo-climate reconstruction from stable isotope variations in speleothems: a review. Quat. Sci. Rev. 23, 901–918.
McManus, J.F., Bond, G.C., Broecker, W.S., Johnsen, S., Labeyrie, L., Higgins, S., 1994. High-resolution climate records from the North Atlantic during the last interglacial. Nature 371, 326–329.
McManus, J.F., Francois, R., Gherardi, J.M., Keigwin, L.D., Brown-Leger, S., 2004. Collapse and rapid resumption of Atlantic meridional circulation linked to deglacial climate changes. Nature 428, 834–837.
Medina-Elizalde, M., 2013. A global compilation of coral sea-level benchmarks: implications and new challenges. Earth Planet. Sci. Lett. 362, 310–318.
Mokeddem, Z., McManus, J.F., Oppo, D.W., 2014. Oceanographic dynamics and the end of the last interglacial in the subpolar North Atlantic. Proc. Natl. Acad. Sci. Unit. States Am. 111, 11263–11268.
Mudelsee, M., 2000. Ramp function regression: a tool for quantifying climate transitions[J]. Comput. Geosci. 26 (3), 293–307.
O'Neil, J.R., 1986. Theoretical and experimental aspects of isotopic fractionation. Rev. Mineral. 16, 1–40.
O'Neil, J.R., Clayton, R.N., Mayeda, T.K., 1969. Oxygen isotope fractionation in Divalent metal carbonates. J. Chem. Phys. 51, 5547–5558.
Oppo, D.W., Horowitz, M., Lehman, S.J., 1997. Marine core evidence for reduced deep water production during Termination II followed by a relatively stable substage 5e (Eemian). Paleoceanography 12, 51–63.
Peltier, W.R., 2004. Global glacial isostasy and the surface of the ice-age Earth: the ICE-5G (VM2) model and GRACE. Annu. Rev. Earth Planet Sci. 32, 111–149.
Regattieri, E., Zanchetta, G., Drysdale, R.N., Isola, I., Hellstrom, J.C., Roncioni, A., 2014. A continuous stable isotope record from the penultimate glacial maximum to the Last Interglacial (159–121 ka) from Tana Che Urla Cave (Apuan Alps, central Italy). Quat. Res. 82, 450–461.
Regattieri, E., Zanchetta, G., Drysdale, R.N., Isola, I., Woodhead, J.D., Hellstrom, J.C.,

Giaccio, B., Greig, A., Baneschi, I., Dotsika, E., 2016. Environmental variability between the penultimate deglaciation and the mid Eemian: insights from Tana che Urla (central Italy) speleothem trace element record. Quat. Sci. Rev. 152, 80–92.

Risebrobakken, B., Balbon, E., Dokken, T., Jansen, E., Kissel, C., Labeyrie, L., Richter, T., Senneset, L., 2006. The penultimate deglaciation: high-resolution paleoceanographic evidence from a north–south transect along the eastern Nordic Seas. Earth Planet. Sci. Lett. 241, 505–516.

Sarnthein, M., Tiedemann, R., 1990. Younger Dryas-style cooling events at glacial terminations I-VI at ODP site 658: associated benthic $\delta^{13}C$ anomalies constrain meltwater hypothesis. Paleoceanography 5, 1041–1055.

Scholz, D., Hoffmann, D.L., 2011. StalAge—An algorithm designed for construction of speleothem age models. Quat. Geochronol. 6, 369–382.

Shackleton, N.J., 2000. The 100,000-year ice-age cycle Identiþed and found to Lag temperature, carbon Dioxide, and orbital Eccentricity. Science 289, 1897–1902.

Sima, A., Paul, A., Schulz, M., 2004. The Younger Dryas—an intrinsic feature of late Pleistocene climate change at millennial timescales. Earth Planet. Sci. Lett. 222, 741–750.

Skinner, L.C., Shackleton, N.J., 2006. Deconstructing Terminations I and II: revisiting the glacioeustatic paradigm based on deep-water temperature estimates. Quat. Sci. Rev. 25, 3312–3321.

Spratt, R.M., Lisiecki, L.E., 2016. A Late Pleistocene sea level stack. Clim. Past 12, 1079–1092.

Stager, J.C., Ryves, D.B., Chase, B.M., Pausata, F.S., 2011. Catastrophic drought in the Afro-Asian monsoon region during Heinrich event 1. Science 331 (6022), 1299–1302.

Tan, M., 2014. Circulation effect: response of precipitation δ18O to the ENSO cycle in monsoon regions of China. Clim. Dyn. 42, 1067–1077.

Tremaine, D.M., Froelich, P.N., Wang, Y., 2011. Speleothem calcite farmed in situ: modern calibration of δ18O and δ13C paleoclimate proxies in a continuously-monitored natural cave system. Geochem. Cosmochim. Acta 75 (17), 4929–4950.

Tzedakis, P.C., Drysdale, R.N., Margari, V., Skinner, L.C., Menviel, L., Rhodes, R.H., Taschetto, A.S., Hodell, D.A., Crowhurst, S.J., Hellstrom, J.C., Fallick, A.E., Grimalt, J.O., McManus, J.F., Martrat, B., Mokeddem, Z., Parrenin, F., Regattieri, E., Roe, K., Zanchetta, G., 2018. Enhanced climate instability in the north Atlantic and southern Europe during the last interglacial. Nat. Commun. 9 (1), 4235.

Wang, P.X., Bradshaw, M., Ganzei, S.S., Tsukawaki, S., Binhassan, K., Hantoro, W.S., Poobrasert, S., Burne, R., Zhao, Q.H., Kagami, H., 1997. West Pacific marginal seas during Last Glacial Maximum: Amplification of environmental signals and its impact on monsoon climate. In: Wang, Berggren (Ed.), Proceedings of 30th International Geological Congress, vol. 13. VSP, Utrecht, the Netherlands, pp. 65–86.

Wang, Y., Cheng, H., Edwards, R.L., An, Z., Wu, J., Shen, C.-C., Dorale, J., 2001. A high-resolution absolute-dated late Pleistocene Monsoon record from Hulu Cave, China. Science 294, 2345–2348.

Wang, Y., Cheng, H., Edwards, R.L., He, Y., Kong, X., An, Z., Wu, J., Kelly, M.J., Dykoski, C.A., Li, X., 2005. The Holocene Asian monsoon: links to solar changes and North Atlantic climate. Science 308, 854–857.

Wang, Y., Cheng, H., Edwards, R.L., Kong, X., Shao, X., Chen, S., Wu, J., Jiang, X., Wang, X., An, Z., 2008. Millennial- and orbital-scale changes in the East Asian monsoon over the past 224,000 years. Nature 451, 1090–1093.

Wang, Q., Zhou, H., Cheng, K., Chi, H., Shen, C.-C., Wang, C., Ma, Q., 2016. The climate reconstruction in Shandong Peninsula, northern China, during the last millennium based on stalagmite laminae together with a comparison to δ18O. Clim. Past 12, 871–881.

Yu, G., Xue, B., Liu, J., Chen, X., 2003. LGM lake records from China and an analysis of climate dynamics using a modelling approach. Glob. Planet. Chang. 38, 223–256.

Yuan, D., Cheng, H., Edwards, R.L., Dykoski, C.A., Kelly, M.J., Zhang, M., Qing, J., Lin, Y., Wang, Y., Wu, J., Dorale, J.A., An, Z., Cai, Y., 2004. Timing, duration, and transitions of the last interglacial Asian monsoon. Science 304, 575–578.

Zhang, P., Cheng, H., Edwards, R.L., Chen, F., Wang, Y., Yang, X., Liu, J., Tan, M., Wang, X., Liu, J., An, C., Dai, Z., Zhou, J., Zhang, D., Jia, J., Jin, L., Johnson, K.R., 2008. A test of climate, sun, and culture relationships from an 1810-year Chinese cave record. Science 322, 940–942.